

# Simultaneous Radar and Communications Emissions from a Common Aperture, Part I: Theory

Patrick M. McCormick  
and Shannon D. Blunt  
Radar Systems Lab  
University of Kansas  
Lawrence, KS

Justin G. Metcalf  
Sensors Directorate  
Air Force Research Lab  
Wright-Patterson AFB, OH

**Abstract**—Multi-function RF systems address the growing need to provide greater functionality with fewer hardware and spectral resources. In this vein, a two-stage iterative optimization approach denoted as far-field radiated emission design (FFRED) is developed that is used here to design a set of physical multi-function waveforms that realize far-field radar and communication signals simultaneously from a common antenna array and with the same spectral support. Particular attention is paid to the efficiency of power radiated into the radar and communication spatial directions, peak-to-average-power ratio (PAPR), and the bit error rate (BER) for the communication mode. Experimental demonstration of this joint emission scheme is presented in the companion paper

**Index Terms**—multi-function RF, spectrum sharing, MIMO radar, communications

## I. INTRODUCTION

The increasing competition for precious spectral resources [1]–[3] is serving as a selection pressure to drive innovation. While no “silver bullet” solution to spectral crowding has been discovered, a wide variety of technologies are being developed under the umbrella of spectrum sharing. Spectrum sharing research can be roughly separated into two categories: 1) where the different modalities (e.g. radar and communications) coexist as separate systems that in some way respond/adapt to one another [4]–[11] and 2) where the different modalities represent facets of the same multi-function RF system [12]–[17]. The former is an interference mitigation problem that could employ dynamic spectral sensing and access, possibly combined with adaptive cancellation. In contrast, the latter represents a co-design paradigm in which the available degrees of freedom are employed to realize more than one objective, often through some form of waveform diversity [18], [19].

This work addresses the co-design problem by formulating the means to emit radar and communication signals simultaneously from the same antenna array aperture with the same spectral support. In so doing, these modes share time, spectrum, and transmit hardware, thereby relieving pressures on the resource management timeline [20], spectral allocation [2], and system requirements [12]. Specifically, this approach relies on a space-division multiple-access (SDMA) type of framework in which the radar and communication signals are concurrently generated in the far-field based on the free-space combination of waveforms emitted from a common antenna

array (see Fig. 1). This arrangement is a form of MIMO beam pattern design [21]–[25] with the particular requirement that the individual waveforms be physically realizable by a high-power transmitter; i.e. be constant amplitude and well-contained spectrally (see [11], [26], [27]). Moreover, beyond the task of realizing a desired spatial power allocation, the problem of generating dual radar and communication beams necessitates design of the resulting far-field emissions that possess physical attributes of useful radar waveforms [19], [28] and communication signals [29].

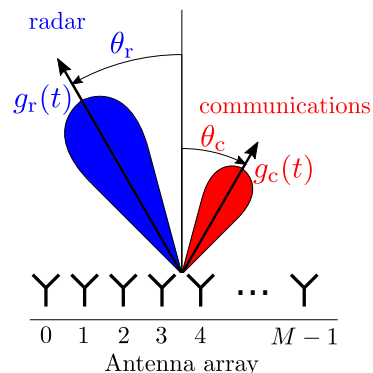


Fig. 1. Simultaneous emission of radar and communication signals from a common antenna array

Here we present a two-stage optimization procedure denoted as far-field radiated emission design (FFRED) that enables generation of arbitrary physical signals as a function of spatial angle and time via a MIMO transmit implementation. It is observed that a side-effect of this design procedure is that the time-domain signals in the spatial sidelobe directions (i.e. where no emission is intended) are naturally uncorrelated with the desired radar and communication signals. Further, in the companion paper [30] this design framework is demonstrated experimentally using an Air Force Research Lab (AFRL) radar testbed.

## II. FAR-FIELD RADIATED EMISSION DESIGN (FFRED)

The FFRED approach generates a set of FM waveforms that, when simultaneously emitted from an antenna array in a MIMO arrangement, combine in the far-field to realize

a desired radar waveform in one spatial direction and an information-bearing communication signal in another direction. Here it is assumed that the primary function of the antenna is to enable a pulsed radar emission while a secondary (and lower power) communication function emits a separate signal concurrently during the radar pulsewidth and with the same bandwidth. While the communication beam does represent a loss in transmit power for the radar (which will translate to reduced receive SNR and thus degraded radar sensitivity), this manner of joint design does allow for the communication signal data rate to scale with the available bandwidth.

### A. Signal Model

Consider an  $M$  element ideal uniform-linear array (ULA) with inter-element spacing  $d$ . Invoking the narrowband assumption, the far-field radar and communication signals must respectively satisfy the constraints

$$\sum_{m=0}^{M-1} s_m(t) \exp\left(jm \frac{2\pi}{\lambda} d \sin \theta_r\right) = g_r(t) \quad (1)$$

and

$$\sum_{m=0}^{M-1} s_m(t) \exp\left(jm \frac{2\pi}{\lambda} d \sin \theta_c\right) = g_c(t) \quad (2)$$

where  $\lambda$  is the free space wavelength of the center frequency  $f_c$ , the waveform emitted by the  $m$ th element is  $s_m(t)$ , and  $g_r(t)$  and  $g_c(t)$  are the desired far-field radar and communication signals to be emitted in spatial directions  $\theta_r$  and  $\theta_c$ , respectively. Discretizing  $s_m(t)$ ,  $g_r(t)$ , and  $g_c(t)$  into length- $N$  vectors, accounting for adequate “over-sampling” with respect to 3 dB bandwidth [11], [26], [27] to maintain sufficient fidelity for physical realization, (1) and (2) can be rewritten as

$$\mathbf{v}^H(\theta_r) \mathbf{S} = \mathbf{g}_r^T \quad (3)$$

and

$$\mathbf{v}^H(\theta_c) \mathbf{S} = \mathbf{g}_c^T. \quad (4)$$

Here  $\mathbf{S} = [\mathbf{s}_0 \ \mathbf{s}_1 \ \dots \ \mathbf{s}_{M-1}]^T$  is an  $M \times N$  matrix comprised of the  $M$  discretized waveforms,  $\mathbf{g}_r$  and  $\mathbf{g}_c$  are  $N \times 1$  vectors of the desired radar and communications signals, and  $\mathbf{v}(\theta)$  is the spatial steering vector for direction  $\theta$  defined as

$$\mathbf{v}(\theta) = \left[ 1 \ \exp\left(-j \frac{2\pi}{\lambda} d \sin \theta\right) \ \dots \ \exp\left(-j(M-1) \frac{2\pi}{\lambda} d \sin \theta\right) \right]^T. \quad (5)$$

The constraints of (3) and (4) can be combined as

$$\mathbf{C}^H \mathbf{S} = \mathbf{G}, \quad (6)$$

where

$$\mathbf{C} = \left[ \mathbf{v}(\theta_r) \ \mathbf{v}(\theta_c) \right] \quad (7)$$

contains the spatial steering vectors and

$$\mathbf{G} = \left[ \mathbf{g}_r \ \mathbf{g}_c \right]^T \quad (8)$$

contains the discretized far-field signals.

### B. Optimality

The optimal waveform matrix  $\mathbf{S}$  (in a minimum norm sense) can be found by solving the minimum-norm optimization problem

$$\begin{aligned} & \underset{\mathbf{S}}{\text{minimize}} \quad \|\mathbf{S}\|_F^2 \\ & \text{subject to} \quad \mathbf{C}^H \mathbf{S} = \mathbf{G} \end{aligned} \quad (9)$$

where  $\|\bullet\|_F^2$  is the squared-Frobenius normalization. The optimization problem in (9) is convex and has the closed-form solution [31]

$$\mathbf{S}_* = \mathbf{C}(\mathbf{C}^H \mathbf{C})^{-1} \mathbf{G}. \quad (10)$$

This waveform matrix is optimal in the sense that all of the energy in the resulting waveforms is used to achieve the constraint (6). However, the solution  $\mathbf{S}_*$  in (10) usually has an unacceptable peak-to-average power ratio (PAPR) that precludes the use of high power amplifiers (HPAs) employed in most radar systems that operate in saturation. From this perspective it is instructive to reconsider what is actually optimal within the context of a physical system.

Arguably a better metric for optimality is power efficiency, which enables maximization of “energy on target” for the radar function. Under this condition an optimization method is presented that facilitates constant amplitude FM waveforms that are amenable to the HPA. The modified optimization problem is

$$\begin{aligned} & \underset{\mathbf{S}}{\text{minimize}} \quad \|\mathbf{S}\|_F^2 \\ & \text{subject to} \quad \mathbf{C}^H \mathbf{S} = \mathbf{G} \\ & \quad |s_m(n)| = |s_p(q)| \text{ for } n, q = 0, \dots, N-1 \\ & \quad \quad \quad m, p = 0, \dots, M-1 \end{aligned} \quad (11)$$

where  $s_m(n)$  is the  $n$ th time sample of the  $m$ th waveform.

### C. Utilization of Null Space and Power Efficiency

To solve (11), the null space of steering vector matrix  $\mathbf{C}$  must be used to form a spatial orthogonal complement matrix  $\mathbf{S}_\perp$  such that the summation

$$\tilde{\mathbf{S}} = \mathbf{S}_* + \mathbf{S}_\perp \quad (12)$$

contains  $M$  discretized waveforms that are constant amplitude. Because the null space of  $\mathbf{C}$  is used to construct  $\mathbf{S}_\perp$ , we have

$$\mathbf{C}^H \mathbf{S}_\perp = \mathbf{0}_{2 \times 1} \quad (13)$$

and thus there is no interference produced in the desired radar and communications directions. Further, since  $\mathbf{S}_*$  and  $\mathbf{S}_\perp$  are orthogonal, the average power in  $\tilde{\mathbf{S}}$  is the summation

$$\gamma^2 = \rho_* + \rho_\perp \quad (14)$$

where  $\rho_*$  and  $\rho_\perp$  are the average power in  $\mathbf{S}_*$  and  $\mathbf{S}_\perp$ , respectively, defined as

$$\rho_* = \frac{1}{MN} \|\mathbf{S}_*\|_F^2 \quad (15)$$

and

$$\rho_\perp = \frac{1}{MN} \|\mathbf{S}_\perp\|_F^2. \quad (16)$$

Since  $\rho_*$  is a fixed amount, the amplitude  $\gamma$  directly affects the amount of power emitted into the null space of  $\mathbf{C}$ . Denote the percentage of power emitted into the orthogonal space as

$$\% \rho_{\perp} = \frac{\rho_{\perp}}{\gamma^2} \times 100\%. \quad (17)$$

This power does not contribute to the emissions in the directions  $\theta_r$  and  $\theta_c$  and thus is essentially wasted power. Therefore, there is a trade-off in the efficiency lost by placing power in the orthogonal space relative to the efficiency gained by using constant amplitude waveforms (and the associated use of high-efficiency HPAs in saturation).

### III. REALIZATION OF EMISSION CONSTRAINTS USING ERROR REDUCTION ALGORITHM

The inclusion of the constant amplitude constraint in (11) makes the minimization problem non-convex and thus it must be solved in an iterative manner. A useful approach to address optimization involving two distinct constraints is to alternate between projecting onto a set that satisfies one constraint and projecting onto a set that satisfies the other constraint. If the sets are convex, this approach is known as Projection onto Convex Sets (POCS) [32], [33]. However, the projection onto the set containing all constant amplitude waveform matrices is not convex. In that case, the Error Reduction Algorithm (ERA) [34]–[37] can be used, which can be thought of as POCS with one or more non-convex projections [34], [35]. While convergence to an intersection (or minimum distance point) between the sets cannot be proven for ERA as it can for POCS, the error in ERA can be shown to be a non-increasing sequence [34]–[37].

#### A. FFRED Optimization

Given some constant amplitude initialization  $\tilde{\mathbf{S}}_0$ , the alternating projections procedure alternates between two stages until convergence. The first stage projects onto some set  $A$  that satisfies a constraint using projection operator  $P_A(\bullet)$ . The second stage projects onto some set  $B$  that satisfies another constraint using projector operator  $P_B(\bullet)$ . For the scenario described in this paper, set  $A$  satisfies the constraint  $\mathbf{C}^H \mathbf{S} = \mathbf{G}$  from (6) and set  $B$  satisfies the constant amplitude constraint. The procedure is summarized in Algorithm 1.

ALGORITHM 1: Alternating Projections

Initialize:  $\tilde{\mathbf{S}}_0, i = 0$

**repeat**

$$\mathbf{S}_i = P_A(\tilde{\mathbf{S}}_i)$$

$$\tilde{\mathbf{S}}_{i+1} = P_B(\mathbf{S}_i)$$

$$i = i + 1$$

**until** sufficiently converged

The projections are defined as the minimum change to the input ( $\tilde{\mathbf{S}}_i$  or  $\mathbf{S}_i$ ) such that the corresponding constraint is satisfied. Using this definition, the projections can be defined as optimization problems. For the first stage, the projection

$P_A(\tilde{\mathbf{S}}_i)$  is defined as

$$\begin{aligned} & \underset{\mathbf{S}_i}{\text{minimize}} \quad \left\| \tilde{\mathbf{S}}_i - \mathbf{S}_i \right\|_F^2 \\ & \text{subject to} \quad \mathbf{C}^H \mathbf{S}_i = \mathbf{G} \end{aligned} \quad (18)$$

The solution to (18) is

$$\mathbf{S}_i = \mathbf{P}_{\perp} \tilde{\mathbf{S}}_i + \mathbf{S}_{\star} \quad (19)$$

where  $\mathbf{P}_{\perp}$  is the projection matrix

$$\mathbf{P}_{\perp} = \mathbf{I}_M - \mathbf{C} (\mathbf{C}^H \mathbf{C})^{-1} \mathbf{C}^H \quad (20)$$

with  $\mathbf{I}_M$  the  $M \times M$  identity matrix. Likewise, the second stage projection  $P_B(\mathbf{S}_i)$  can be represented as

$$\begin{aligned} & \underset{\tilde{\mathbf{S}}_{i+1}}{\text{minimize}} \quad \left\| \tilde{\mathbf{S}}_{i+1} - \mathbf{S}_i \right\|_F^2 \\ & \text{subject to} \quad |\tilde{s}_{m,i+1}(n)| = \gamma \quad \text{for } n = 0, \dots, N-1 \\ & \quad \quad \quad m = 0, \dots, M-1 \end{aligned} \quad (21)$$

for some real amplitude  $\gamma$ . The solution to (21) is

$$\tilde{\mathbf{S}}_{i+1} = \gamma \exp \{j \angle(\mathbf{S}_i)\} \quad (22)$$

where  $\angle(\bullet)$  extracts the phase of the argument. The value of amplitude  $\gamma$  can be determined from (14) and (17) by setting a desired percent orthogonal power  $\% \rho_{\perp}$  as

$$\gamma = \left( \frac{\rho_{\star}}{1 - \% \rho_{\perp}} \right)^{1/2} \quad (23)$$

Note that the desired percent orthogonal power  $\% \rho_{\perp}$  is only achieved if the algorithm converges onto a solution that satisfies both constraints. For certain constraints  $\mathbf{C}$  and  $\mathbf{G}$  and initialization  $\mathbf{S}_0$  there exists a minimum percent orthogonal power necessary to achieve a constant amplitude solution, and thus care must be taken when choosing  $\gamma$ . If  $\gamma$  is selected based on a desired percent orthogonal power below this minimum percentage, a solution that satisfies both constraints cannot be found because the sets onto which projections are performed do not intersect. For the simulations that follow, various desired percent orthogonal powers  $\% \rho_{\perp}$  are used to establish the amplitude  $\gamma$ .

The waveform matrix after the second stage can be represented as a summation of matrices similar to (12) as

$$\tilde{\mathbf{S}}_i = \mathbf{S}_{\perp,i} + \mathbf{S}_{\star} + \mathbf{S}_{\text{int},i} \quad (24)$$

where  $\mathbf{S}_{\perp,i} = \mathbf{P}_{\perp} \tilde{\mathbf{S}}_i$ . The term  $\mathbf{S}_{\text{int},i}$  is a ‘‘self-interference’’ matrix that arises after the projection in (21) due to deviation from the constraint  $\mathbf{C}^H \mathbf{S} = \mathbf{G}$ . Ideally,  $\mathbf{S}_{\text{int},i}$  would contain zero power and therefore (24) would reduce to the form in (12). Thus reduction of this self-interference power is necessary to find a solution that satisfies both constraints.

The two-stage iterative optimization process is shown in Fig. 2 where Stage 1 and Stage 2 are the projections defined in (18) and (21), respectively. The algorithm iterates until some convergence criteria is met. The error reduction property for this problem comes in the form of

$$\dots \leq \left\| \tilde{\mathbf{S}}_{i+1} - \mathbf{S}_{i+1} \right\|_F^2 \leq \left\| \tilde{\mathbf{S}}_{i+1} - \mathbf{S}_i \right\|_F^2 \leq \left\| \tilde{\mathbf{S}}_i - \mathbf{S}_i \right\|_F^2 \leq \dots \quad (25)$$

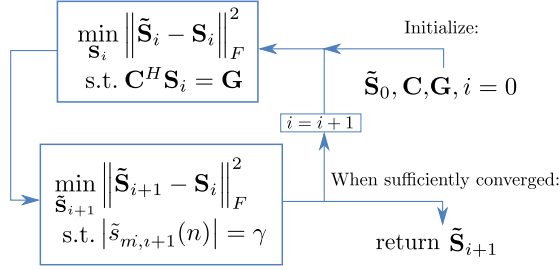


Fig. 2. Flowchart of emission optimization algorithm

where the square-Euclidean distance between the successive waveform matrices is a non-increasing sequence.

### B. Peak-to-average power ratio vs. self-interference

The output of Stage 1 ( $\mathbf{S}_i$ ) satisfies the constraint  $\mathbf{C}^H \mathbf{S} = \mathbf{G}$  but does not necessarily satisfy the constant modulus constraint. Monitoring the convergence of the peak-to-average power ratio (PAPR) at the output of Stage 1 is therefore a good measure of the quality of the waveform matrix at iteration  $i$ . The PAPR ratio of the waveform matrix at the output of Stage 1 at the  $i$ th iteration is

$$PAPR_i = \frac{\max_{m,n} |s_{m,i}(n)|^2}{\frac{1}{MN} \|\mathbf{S}_i\|_F^2}. \quad (26)$$

Likewise, the output of Stage 2 ( $\tilde{\mathbf{S}}_i$ ) satisfies the constant modulus constraint but does not necessarily satisfy the constraint  $\mathbf{C}^H \mathbf{S} = \mathbf{G}$  due to the presence of the self-interference matrix  $\mathbf{S}_{\text{int},i}$ . Thus the self-interference power after Stage 2 at iteration  $i$  is defined as

$$\rho_{\text{int},i} = \frac{1}{MN} \|\mathbf{S}_{\text{int},i}\|_F^2. \quad (27)$$

Using this quantity, a signal to self-interference power ratio at iteration  $i$  can be defined as

$$SIR_i = \frac{\rho_\star}{\rho_{\text{int},i}}. \quad (28)$$

As the interference power  $\rho_{\text{int},i}$  approaches 0, the signal to self-interference power ratio approaches infinity, so it is advantageous to monitor the inverse ratio  $[SIR_i]^{-1}$ . Monitoring the reduction of this self-interference power at the output of Stage 2 gives insight into how the algorithm converges. If the self-interference power after Stage 2 is zero (infinite  $SIR_i$ ), then both constraints are met and a solution is obtained. Since the output of Stage 2 is always a constant modulus result, the final converged solution may contain some self-interference depending on the value of  $\gamma$ .

## IV. SIMULTANEOUS RADAR-COMMS SIMULATION RESULTS

Consider an  $M = 16$  element ULA with element spacing  $d = \lambda/2$ . We wish simultaneously to emit a radar beam towards boresight ( $\theta_r = 0^\circ$ ) and a communications beam towards  $\theta_c = 45^\circ$  with 10 dB less power than the radar

beam. The radar waveform is an up-chirped linear frequency-modulated (LFM) waveform with time-bandwidth product  $BT = 64$ , for 3 dB bandwidth  $B$  and pulsewidth  $T$ .

The communication modulation is chosen to have a Quadrature Phase-Shift Keying (QPSK) structure (2 bits per symbol). The symbols are convolved with a Square-Root Raised-Cosine (SRRC) shaping filter to constrain the bandwidth of the communication signal. This shaping filter spans 10 symbols. For  $BT = 64$ , the pulsewidth can accommodate 54 symbols (due to the length of the shaping filter), thus enabling 108 bits to be transmitted per pulse. A total of 1000 Monte Carlo trials were performed to generate different bit sequences for the optimization. Note that due to sufficient “over-sampling” of the desired radar and communications signals  $g_r(t)$  and  $g_c(t)$ , the optimized waveform matrix retains sufficient spectral containment such that the final version can be readily converted into a set of FM waveforms [26].

The algorithm was run for desired percent orthogonal powers of 10%, 20%, 30%, 40% and 50%, where the amplitude  $\gamma$  for each case was calculated using (23). Recall that for each initialization there exists a minimum percent orthogonal power that is necessary to satisfy the emission constraints, and thus the final solution may have a non-zero  $\mathbf{S}_{\text{int},i}$ . For each trial, the waveform matrix initializations  $\tilde{\mathbf{S}}_0$  were obtained by random generating Polyphase-Coded Frequency Modulated (PCFM) waveforms [26].

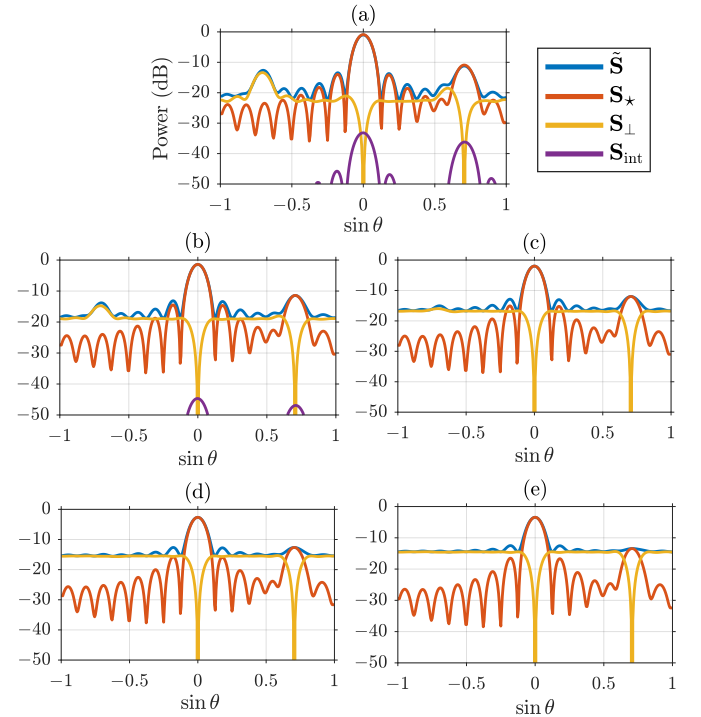


Fig. 3. Average beampatterns of optimized emission (blue), minimum-norm emission (red), orthogonal emission (yellow), and interference emission (purple) for (a) 10% (b) 20% (c) 30% (d) 40% and (e) 50% desired orthogonal powers.

Fig. 3 shows the final average beampatterns at the output of Stage 2 ( $\tilde{\mathbf{S}}_i$ ) after 2000 iterations of the algorithm for the five orthogonal power settings averaged over 1000 Monte Carlo trials. The beampatterns of components  $\mathbf{S}_*$  (red),  $\mathbf{S}_\perp$  (yellow), and  $\mathbf{S}_{\text{int}}$  (purple) of the final waveform matrix  $\tilde{\mathbf{S}}$  (blue) are shown. The scaling of the beampattern is such that 0 dB is the peak power that can be emitted from the array. Note how the orthogonal beampattern has nulls in the directions of the radar and communication beams. Also note how the sidelobe floor raises with increasing orthogonal power, which is also accompanied by an attendant reduction in the peak values of the radar and communication beams. In Figs. 3(a) and 3(b) the appearance of self-interference (purple) signifies that the specified orthogonal powers of 10% and 20% are not large enough to find a solution that satisfies both constraints.

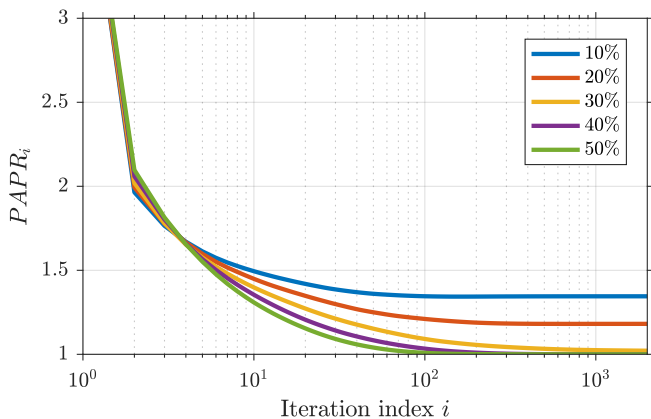


Fig. 4. Peak-to-average power ratio versus iteration  $i$  after Stage 1 (1000 Monte Carlo trials).

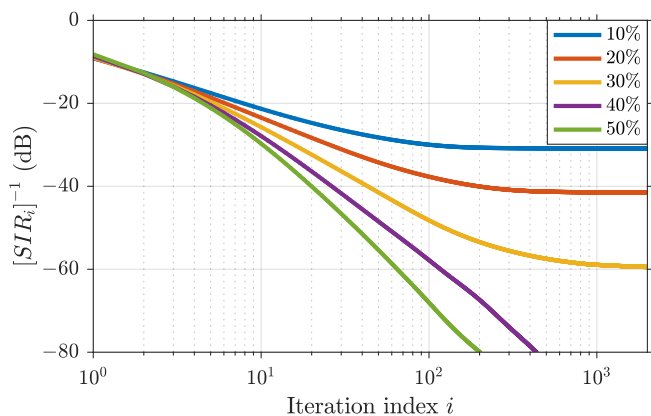


Fig. 5. Inverse signal to self-interference power ratio versus iteration  $i$  after Stage 2 (1000 Monte Carlo trials).

Fig. 4 shows the PAPR from (26) after Stage 1 ( $\mathbf{S}_i$ ) at each iteration. While the 40% and 50% cases clearly converge to meet the constant amplitude constraint, the cases of 10%, 20%, and 30% do not (though the latter is close). Fig. 5 illustrates the inverse signal to self-interference power via (28) versus iteration  $i$  at the output of Stage 2. As expected, the 10%, 20%, and 30% cases converge onto an emission with non-

zero self-interference, though the level of interference is quite small and may be acceptable in some cases.

The lack of convergence in the cases of  $\% \rho_\perp = \{10\%, 20\%, 30\%\}$  show that the amount of power allowed in the orthogonal space is insufficient to obtain a solution that satisfies the constraints of both stages. Note that this outcome is dependent on the particular set of parameters and constraints ( $\theta_r$ ,  $\theta_c$ , relative power of 10 dB, communications modulation and shaping filter, etc.) and is not indicative of the behavior for all optimization scenarios.

Fig. 6 shows the bit error rate (BER) versus  $\sin \theta$  for the five orthogonal power scenarios and the minimum-norm solution. Maximum-likelihood was used to demodulate the communication signal and the QPSK constellation was phase rotated to achieve the minimum BER for each angle. No noise was added and therefore the BER curves are based solely on the spatial diversity of the emission. The  $\mathbf{S}_*$  curve demonstrates the interference between the radar and communications functions for the minimum-norm solution, where it is observed that the data can only be demodulated in the nulls of the radar transmission. Also, the width of the BER curve in the direction of communication ( $\sin \theta_c = 0.7071$ ) depends on the amount of orthogonal power. Clearly, the FFRED approach eliminates interference from the strong, collocated radar waveform in the desired direction for the communication function.

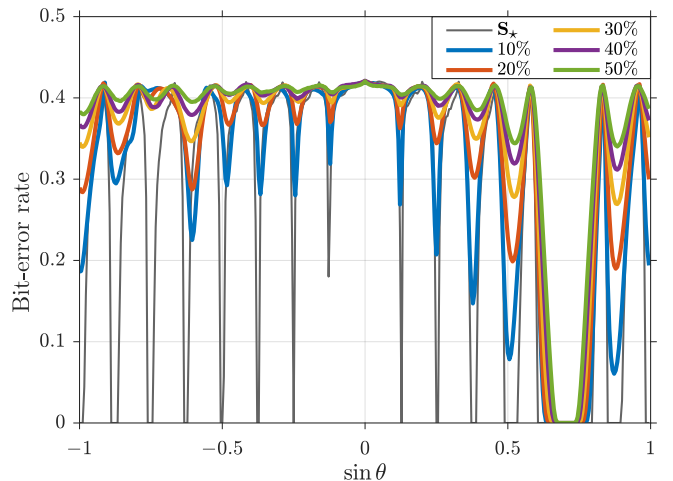


Fig. 6. Bit-error rate versus  $\sin \theta$  for QPSK-modulated communications signal emitted toward  $\sin \theta_c = 0.7071$ .

## V. CONCLUSION

A new two-stage, iterative algorithm denoted as far-field radiated emission design (FFRED) was developed to realize arbitrary emissions using a MIMO transmit structure. The new approach supplements the minimum-norm constrained solution with a spatially orthogonal component in order to improve power efficiency of the resulting set of multi-function waveforms. The convergence, sidelobe structure, and communication demodulation of the theoretical emissions have been examined. Finally, it was shown that the designed

communication emissions do not suffer from interference from the radar emissions in the mainbeam direction of the communication signal. Experimental validation of the FFRED algorithm is provided in the companion paper [30].

#### ACKNOWLEDGMENT

This work was supported by a subcontract with Matrix Research, Inc. for research sponsored by AFRL under Prime Contract # FA8650-14-D-1722.

#### REFERENCES

- [1] J. Mitola, J. Guerci, J. Reed, Y. D. Yao, Y. Chen, T. C. Clancy, J. Dwyer, H. Li, H. Man, R. McGwier, and Y. Guo, "Accelerating 5G QoE via public-private spectrum sharing," *IEEE Commun. Mag.*, vol. 52, no. 5, pp. 77–85, May 2014.
- [2] H. Griffiths, L. Cohen, S. Watts, E. Mokole, C. Baker, M. Wicks, and S. Blunt, "Radar spectrum engineering and management: Technical and regulatory issues," *Proc. IEEE*, vol. 103, no. 1, pp. 85–102, Jan 2015.
- [3] H. Griffiths, S. Blunt, L. Cohen, and L. Savy, "Challenge problems in spectrum engineering and waveform diversity," in *2013 IEEE Radar Conference*, April 2013, pp. 1–5.
- [4] L. S. Wang, J. P. Mcgeehan, C. Williams, and A. Doufexi, "Application of cooperative sensing in radar-communications coexistence," *IET Communications*, vol. 2, no. 6, pp. 856–868, July 2008.
- [5] J. T. Johnson, C. J. Baker, H. Wang, L. Ye, and C. Zhang, "Assessing the potential for spectrum sharing between communications and radar systems in the L-band portion of the RF spectrum allocated to radar," in *2014 International Conference on Electromagnetics in Advanced Applications (ICEAA)*, Aug 2014, pp. 331–334.
- [6] A. Martone, K. Sherbondy, K. Ranney, and T. Dogaru, "Passive sensing for adaptable radar bandwidth," in *2015 IEEE Radar Conference*, May 2015, pp. 280–285.
- [7] R. A. Romero and K. D. Shepherd, "Friendly spectrally shaped radar waveform with legacy communication systems for shared access and spectrum management," *IEEE Access*, vol. 3, pp. 1541–1554, 2015.
- [8] J. G. Metcalf, C. Sahin, S. D. Blunt, and M. Rangaswamy, "Analysis of symbol-design strategies for intrapulse radar-embedded communications," *IEEE Trans. Aerosp. Electron. Syst.*, vol. 51, no. 4, pp. 2914–2931, Oct 2015.
- [9] G. Meager, R. A. Romero, and Z. Staples, "Estimation and cancellation of high powered radar interference for communication signal collection," in *2016 IEEE Radar Conference*, May 2016, pp. 1–4.
- [10] F. Hesar and S. Roy, "Spectrum sharing between a surveillance radar and secondary Wi-Fi networks," *IEEE Trans. Aerosp. Electron. Syst.*, vol. 52, no. 3, pp. 1434–1448, June 2016.
- [11] P. M. McCormick, S. D. Blunt, and J. G. Metcalf, "Wideband MIMO frequency modulated emission design with space-frequency nulling," *IEEE J. Sel. Topics Signal Process.*, vol. 11, no. 2, pp. 363–378, March 2017.
- [12] G. C. Tavik, C. L. Hilterbrick, J. B. Evins, J. J. Alter, J. G. Crnkovich, J. W. de Graaf, W. Habicht, G. P. Hrin, S. A. Lessin, D. C. Wu, and S. M. Hagewood, "The advanced multifunction RF concept," *IEEE Trans. Microw. Theory Tech.*, vol. 53, no. 3, pp. 1009–1020, March 2005.
- [13] S. D. Blunt, M. R. Cook, and J. Stiles, "Embedding information into radar emissions via waveform implementation," in *2010 International Waveform Diversity and Design Conference*, Aug 2010, pp. 195–199.
- [14] D. Garmatyuk, J. Schuerger, and K. Kauffman, "Multifunctional software-defined radar sensor and data communication system," *IEEE Sensors J.*, vol. 11, no. 1, pp. 99–106, Jan 2011.
- [15] A. Hassanien, M. G. Amin, Y. D. Zhang, and F. Ahmad, "Dual-function radar-communications: Information embedding using sidelobe control and waveform diversity," *IEEE Trans. Signal Process.*, vol. 64, no. 8, pp. 2168–2181, April 2016.
- [16] B. Ravenscroft, P. M. McCormick, S. D. Blunt, J. Jakobosky, and J. G. Metcalf, "Tandem-hopped OFDM communications in spectral gaps of FM noise radar," in *2017 IEEE Radar Conference*, May 2017.
- [17] C. Sahin, J. Jakobosky, P. M. McCormick, J. G. Metcalf, and S. D. Blunt, "A novel approach for embedding of communication symbols into radar waveforms," in *2017 IEEE Radar Conference*, May 2017.
- [18] M. Wicks and E. Mokole, *Principles of waveform diversity and design*. The Institution of Engineering and Technology, 2011.
- [19] S. D. Blunt and E. L. Mokole, "Overview of radar waveform diversity," *IEEE Aerosp. Electron. Syst. Mag.*, vol. 31, no. 11, pp. 2–42, November 2016.
- [20] M. Scharrenbroich and M. Zatman, "Joint radar-communications resource management," in *2016 IEEE Radar Conference*, May 2016, pp. 1–6.
- [21] D. R. Fuhrmann and G. S. Antonio, "Transmit beamforming for MIMO radar systems using signal cross-correlation," *IEEE Trans. Aerosp. Electron. Syst.*, vol. 44, no. 1, pp. 171–186, January 2008.
- [22] P. Stoica, J. Li, and X. Zhu, "Waveform synthesis for diversity-based transmit beampattern design," *IEEE Trans. Signal Process.*, vol. 56, no. 6, pp. 2593–2598, June 2008.
- [23] H. He, P. Stoica, and J. Li, "Wideband MIMO systems: Signal design for transmit beampattern synthesis," *IEEE Trans. Signal Process.*, vol. 59, no. 2, pp. 618–628, Feb 2011.
- [24] B. Friedlander, "On transmit beamforming for MIMO radar," *IEEE Trans. Aerosp. Electron. Syst.*, vol. 48, no. 4, pp. 3376–3388, October 2012.
- [25] O. Aldayel, V. Monga, and M. Rangaswamy, "Tractable MIMO beampattern design under constant modulus waveform constraint," in *2016 IEEE Radar Conference*, May 2016, pp. 1–6.
- [26] S. D. Blunt, M. Cook, J. Jakobosky, J. D. Graaf, and E. Perrins, "Polyphase-coded FM (PCFM) radar waveforms, Part I: Implementation," *IEEE Trans. Aerosp. Electron. Syst.*, vol. 50, no. 3, pp. 2218–2229, July 2014.
- [27] J. Jakobosky, S. D. Blunt, and B. Himed, "Spectral-shape optimized FM noise radar for pulse agility," in *2016 IEEE Radar Conference*, May 2016, pp. 1–6.
- [28] N. Levanon and E. Mozeson, *Radar signals*. John Wiley & Sons, 2004.
- [29] D. Tse and P. Viswanath, *Fundamentals of wireless communication*. Cambridge university press, 2005.
- [30] P. M. McCormick, A. J. Duly, B. Ravenscroft, J. G. Metcalf, and S. D. Blunt, "Simultaneous radar and communications emission from a common aperture, Part II: Experimentation," in *2017 IEEE Radar Conference*, May 2017.
- [31] S. Boyd and L. Vandenberghe, *Convex optimization*. Cambridge university press, 2004.
- [32] D. Youla, "Generalized image restoration by the method of alternating orthogonal projections," *IEEE Trans. Circuits Syst.*, vol. 25, no. 9, pp. 694–702, Sep 1978.
- [33] D. C. Youla and H. Webb, "Image restoration by the method of convex projections, Part 1: Theory," *IEEE Trans. Med. Imag.*, vol. 1, no. 2, pp. 81–94, Oct 1982.
- [34] A. Levi and H. Stark, "Image restoration by the method of generalized projections with application to restoration from magnitude," in *Acoustics, Speech, and Signal Processing, IEEE International Conference on ICASSP '84.*, vol. 9, Mar 1984, pp. 88–91.
- [35] H. H. Bauschke, P. L. Combettes, and D. R. Luke, "Phase retrieval, error reduction algorithm, and fienuip variants: a view from convex optimization," *JOSA A*, vol. 19, no. 7, pp. 1334–1345, 2002.
- [36] L. K. Patton and B. D. Rigling, "Phase retrieval for radar waveform optimization," *IEEE Trans. Aerosp. Electron. Syst.*, vol. 48, no. 4, pp. 3287–3302, October 2012.
- [37] J. R. Fienup, "Phase retrieval algorithms: a comparison," *Applied optics*, vol. 21, no. 15, pp. 2758–2769, 1982.